Pulsed ultrasound modulated optical tomography with harmonic lock-in holography detection

Haowen Ruan, Melissa L. Mather, and Stephen P. Morgan*

Electrical Systems and Optics Research Division, Faculty of Engineering, University of Nottingham, Nottingham NG7 2RD, UK
**Corresponding author: steve.morgan@nottingham.ac.uk*

Received February 25, 2013; accepted April 3, 2013;
posted June 6, 2013 (Doc. ID 185426); published June 27, 2013

A method that uses digital heterodyne holography reconstruction to extract scattered light modulated by a single-cycle ultrasound (US) burst is demonstrated and analyzed. An US burst is used to shift the pulsed laser frequency by a series of discrete harmonic frequencies which are then locked on a CCD. The analysis demonstrates that the unmodulated light's contribution to the detected signal can be canceled by appropriate selection of the pulse repetition frequency. It is also shown that the modulated signal can be maximized by selecting a pulse sequence which consists of a pulse followed by its inverted counterpart. The system is used to image a 12 mm thick chicken breast with 2 mm wide optically absorbing objects embedded at the midplane. Furthermore, the method can be revised to detect the nonlinear US modulated signal by locking at the second harmonic US frequency.

OCIS codes: (170.0110) Imaging systems; (170.1065) Acousto-optics.
http://dx.doi.org/10.1364/JOSAA.30.001409

1. INTRODUCTION

Due to optical scattering, it is challenging to map the absorption and scattering coefficients deep inside tissue with high resolution and high contrast using optical techniques alone. Ultrasound modulated optical tomography (USMOT), combining optical and ultrasonic techniques, has the potential to provide nonionizing and noninvasive functional imaging of tissue. Coherent light and ultrasound (US) are simultaneously applied to the samples and light that passes through the US focus is phase modulated due to both a change in the refractive index and a change in the displacement of scatterers within the focal volume [1]. This produces a modulated optical speckle pattern at the detector plane. There are a number of approaches to demodulating the speckle pattern. Parallel lock-in detection [2] can be used to lock the US modulated light at a pixelated detector and obtains high signal-to-noise ratio (SNR) due to the large optical acceptance solid angle. Techniques based on digital holography [3] and holography using a photorefractive crystal [4] have also been used to demodulate the speckle pattern. In these methods, the frequency of a reference laser beam is tuned to match the US modulated light frequency and a static hologram of the US modulated light is written onto the camera or photorefractive crystal. One of the major advantages of such approaches is that optical gain is applied to the signal due to interference between the modulated signal and reference beam. Importantly, speckle decorrelation noise can be reduced as the US modulated signal is separated from speckle decorrelation noise in the k-space of the hologram. There has been increasing interest in applying pulsed US to USMOT for both harmonic imaging [5] and time reversal US encoding [6,7]. Other techniques have been applied to detect the US modulated optical signal such as Fabry–Perot interferometry [8,9] and spectral hole burning [10]. All these techniques can be adapted for use with short US pulses [11,12], which enables axial resolution to be obtained through time gating. However, the use of short (wideband) pulses is not ideal for use with narrow band detection as signal energy is lost during the filtering process.

In this paper, we report and analyze a pulsed USMOT technique using a harmonic lock-in technique based on heterodyne holographic reconstruction that can be used to detect light modulated by either the fundamental or second harmonic US. Scattered light is modulated by a single-cycle US burst train, comprised of a series of discrete harmonic frequencies (at the pulse repetition frequency), and is detected using digital holography. The method is useful because the frequencies contained in the response of the lock-in detection matches those of the US modulated light signal. This allows wide band detection of the energy of the US modulated optical pulse, which can improve SNR. Furthermore, the advantages of optical gain, as well as large optical etendue, are inherited from digital holography [3]. The analysis provided in the next section allows the optimum parameters (pulse repetition frequency and reference frequency) to be set. We also demonstrate that this approach can be adapted to image the US modulated optical signal caused by nonlinear propagation of the US. This can reduce the US beam waist at higher harmonic frequencies, reducing sidelobes and improving lateral spatial resolution.

2. SIGNAL PROCESSING THEORY

A. Digital Heterodyne Holography

Detection of the pulsed US modulated optical signal is based on a heterodyne holographic technique [3] (Fig. 1). In the

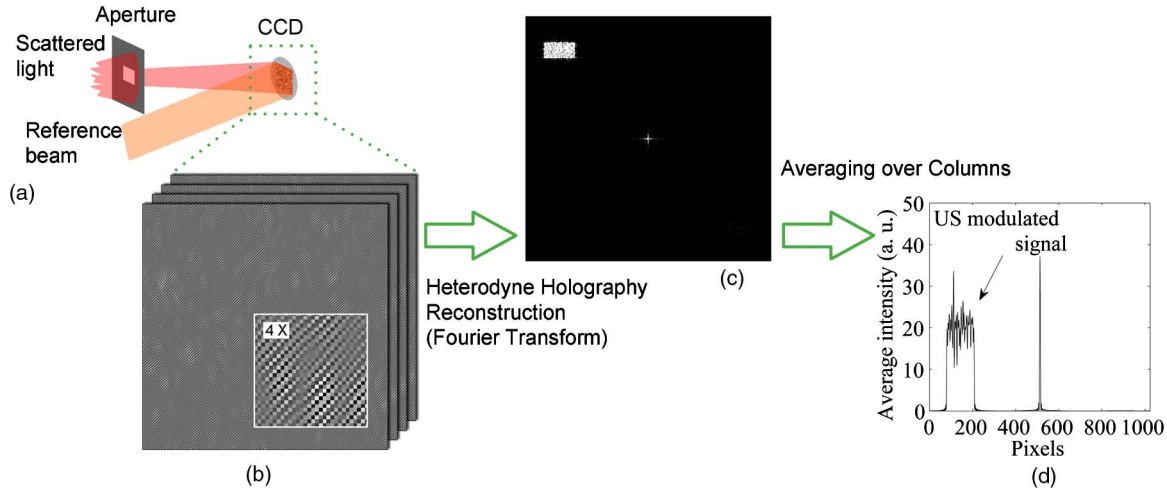

Fig. 1. Digital holography detection. (a) Scattered light from the aperture interferes with the reference at the detector plane; (b) static speckles can be observed corresponding to US modulated light; (c) Fourier transform of (b); and (d) averaging over the rows to obtain the US modulated signal.

linear acoustic regime, light emerging from a scattering medium contains a frequency component at the optical frequency and a component that has been shifted by the US frequency. Scattered light emerging from an aperture situated in front of the camera forms a speckle pattern on the camera. A reference beam at the US shifted optical frequency also illuminates the camera, which means that static interference fringes are formed when the US modulated light from the sample interferes with the reference [Fig. 1(b)]. Unmodulated light at the optical frequency beats with the reference beam at the US frequency and is temporally averaged out at the camera. Taking the Fourier transform of the speckle pattern results in the image of the aperture [Fig. 1(c)], and averaging along the columns enables the US modulated optical signal to be extracted [Fig. 1(d)].

The pulsed USMOT technique analyzed here is based on digital holography and uses pulsed US and synchronized time-gated laser pulses to improve USMOT axial imaging resolution (Fig. 2). The camera is used as a time-integrated detector to average out the dynamic interference fringes due to unmodulated light and to detect the static fringes due to US modulated light. The theoretical derivation shown in this section consists of following steps. First, the general condition to eliminate the unmodulated light is derived, followed by the condition for maximizing the detection of US modulated light. Second, a Fourier series analysis demonstrates that the optimum US pulse sequence that meets these general conditions consists of a train of noninverted and inverted pulses. Finally, the frequency components of the interference signal on the CCD and the pass band of the lock-in detection are compared,

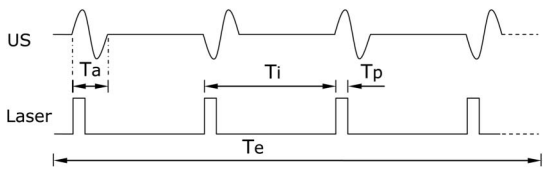

Fig. 2. Pulse sequences for US: noninverted and inverted US pulse train; Laser: laser pulse train. The US and laser are synchronized so that the US pulse arriving at the US focal zone modulates the light at the phases shown. T_a, US pulse duration; T_i, pulse train interval; T_p, laser pulse duration; T_e, exposure time.

demonstrating that the discrete frequency components of the US modulated signals can be locked.

At time t_0, the US pulse arrives at the US transducer focal zone, at which point the synchronized laser pulse is triggered (Fig. 2 shows the timing of the interaction between the US and light at the US focal zone). The optical intensity of the interference between the signal beam and reference beam at one point (approximately one pixel of the camera) on the hologram plane is given by

$$\begin{aligned} I = {} & I_r + I_b + I_m + 2\sqrt{I_r I_b}\cos(2\pi\Delta f t_0 + \Delta\varphi_{rb}) \\ & + 2\sqrt{I_r I_m}\cos[2\pi(\Delta f \pm f_a)t_0 + \Delta\varphi_{rm}] \\ & + 2\sqrt{I_b I_m}\cos(\pm f_a t_0 + \Delta\varphi_{bm}), \end{aligned} \tag{1}$$

where I_r, I_b, and I_m are the light intensity of reference beam, unmodulated light, and modulated light, respectively; f_a is the US frequency; Δf is the frequency difference between the reference beam and the unmodulated laser beam; $\Delta\varphi_{rb}$, $\Delta\varphi_{rm}$, and $\Delta\varphi_{bm}$ are the optical phase differences between the two interfering field components. Here, the reference beam intensity is much higher than the scattered light intensity; therefore, Eq. (1) is approximated to

$$\begin{aligned} I = {} & I_r + 2\sqrt{I_r I_b}\cos(2\pi\Delta f t_0 + \Delta\varphi_{rb}) \\ & + 2\sqrt{I_r I_m}\cos[2\pi(\Delta f \pm f_a)t_0 + \Delta\varphi_{rm}]. \end{aligned} \tag{2}$$

The last two terms represent the AC fringes due to interference between the unmodulated light and the reference beam, and interference between the modulated light and the reference beam. Similarly, at time t_1, when the next US pulse arrives at the same position, the light intensity is given by

$$\begin{aligned} I' = {} & I_r + 2\sqrt{I_r I_b}\cos(2\pi\Delta f t_1 + \Delta\varphi_{rb}) \\ & + 2\sqrt{I_r I_m}\cos[2\pi(\Delta f \pm f_a)t_1 + \Delta\varphi_{rm}]. \end{aligned} \tag{3}$$

The objective is to select pairs of pulses [Eqs. (2) and (3)] that eliminate the contribution of unmodulated light from the detected signal while maximizing the contribution from US

modulated light. In order to cancel the unmodulated light fringes when two light pulses sum up on the camera, the sum of the second terms of both Eqs. (2) and (3) should be zero, which infers

$$2\pi\Delta f(t_1 - t_0) = (2n+1)\pi, \qquad n = 0, 1, 2, \ldots, \tag{4}$$

$$\Delta f = \left(n + \frac{1}{2}\right) f_i, \qquad n = 0, 1, 2, \ldots, \tag{5}$$

where $f_i = 1/T_i$; $T_i = t_1 - t_0$ (Fig. 2). It is interesting to note that the effect of unmodulated light on the detected signal can be eliminated at a given Δf by appropriate selection of the pulse repetition frequency alone.

To maximize the contribution of US modulated light to the detected signal, the sum of the third terms in Eqs. (2) and (3) should be a maximum. This occurs when they are in phase, which infers

$$\begin{aligned} &2\pi(\Delta f \pm f_a)(t_1 - t_0) = 2n\pi, \qquad n \in z; \\ &2\pi\Delta f(t_1 - t_0) \pm 2\pi f_a(t_1 - t_0) = 2n\pi, \end{aligned} \tag{6}$$

where z is the set of integers. In order to both maximize the US modulated signal and cancel the unmodulated light contribution, Eq. (5) needs to be substituted into Eq. (6):

$$\pm 2\pi f_a(t_1 - t_0) = (2n' + 1)\pi - 2n\pi, \qquad n, n' \in z. \tag{7}$$

As f_a is a non-negative frequency, the condition for static fringes due to the US modulated signal, i.e., for maximizing the contribution to the signal from the US modulated signal, can be rewritten as

$$2\pi f_a T_i = (2n+1)\pi, \qquad n = 0, 1, 2, \ldots, \tag{8}$$

$$f_a = \left(n + \frac{1}{2}\right) f_i, \qquad n = 0, 1, 2, \ldots. \tag{9}$$

Equations (8) and (9) indicate that the phase of the US signal at t_1 should be inverted from that at t_0. The condition for maximizing the modulated light is therefore met by the pulse train shown in Fig. 2, where an US pulse is followed by its inverse at a pulse repetition frequency f_i. We now analyze this pulse train in the frequency domain.

It should be noted that the period of the US pulse train is $2T_i$ rather than T_i, as there is one pulse pair in each period. It can be expanded as a Fourier series

$$g(t) = \sum_1^\infty A_n \cos\left(2\pi n \frac{f_i}{2} t\right) + B_n \sin\left(2\pi n \frac{f_i}{2} t\right), \tag{10}$$

where the Fourier amplitude coefficient A_n is given by

$$\begin{aligned} A_n = \frac{1}{\pi}\Bigg\{ &\int_{-\pi}^{-\pi+\frac{a}{b}2\pi} \sin\left[\frac{b}{a}(x+\pi)\right]\cos(nx)\mathrm{d}x \\ &+ \int_0^{\frac{b}{a}2\pi} \sin\left(\frac{b}{a}x + \pi\right)\cos(nx)\mathrm{d}x\Bigg\}, \end{aligned} \tag{11}$$

where $a/b = T_a/(2T_i)$ is the duty cycle of the US pulse pair. A_n can be simplified to

$$\begin{aligned} A_n = \frac{1}{\pi}\Bigg[&\int_0^{\frac{a}{b}2\pi} \sin\left(\frac{b}{a}x\right)\cos(nx - n\pi)\mathrm{d}x \\ &- \int_0^{\frac{b}{a}2\pi} \sin\left(\frac{b}{a}x\right)\cos(nx)\mathrm{d}x\Bigg]; \end{aligned} \tag{12}$$

$$A_n = \frac{1}{\pi}\left\{\int_0^{\frac{a}{b}2\pi} \sin\left(\frac{b}{a}x\right)[\cos(nx - n\pi) - \cos(nx)]\mathrm{d}x\right\}. \tag{13}$$

Similarly,

$$B_n = \frac{1}{\pi}\left\{\int_0^{\frac{a}{b}2\pi} \sin\left(\frac{b}{a}x\right)[\sin(nx - n\pi) - \sin(nx)]\mathrm{d}x\right\}. \tag{14}$$

If n is an even number in Eqs. (13) and (14), $A_n = B_n = 0$, $g(t)$ in Eq. (10) is zero. Therefore, as the Fourier series of the US waveform retains only odd orders, Eq. (10) can be rewritten as

$$g(t) = \sum_1^\infty A_n \cos\left[2\pi\left(n + \frac{1}{2}\right) f_i t\right] + B_n \sin\left[2\pi\left(n + \frac{1}{2}\right) f_i t\right], \quad n = 0, 1, 2, \ldots. \tag{15}$$

Thus, the US signal [Fig. 2 and Eq. (15)] fulfills the condition described in Eq. (9). The synchronized laser pulse train effectively acts as a lock-in detector, which locks the US modulated signal at the US pulse repetition frequency and its harmonics. For a laser pulse train with time interval T_i, the normalized response function of the lock-in detection is the square of the Fourier transform of the laser pulse train (Fig. 2), given by

$$P(f) = \mathrm{sinc}^2(\pi f T_p)\left[\sum_0^\infty \delta(f - nf_i) \otimes \mathrm{sinc}(\pi f T_e)\right]^2, \tag{16}$$

where T_p is the laser pulse width; $\otimes$ denotes convolution. The convolution with $\mathrm{sinc}(\pi f T_e)$ can be ignored in the following analysis, as $T_e \gg T_i$. Therefore, Eq. (16) becomes

$$P(f) = \mathrm{sinc}^2(\pi f T_p) \sum_0^\infty \delta(f - nf_i). \tag{17}$$

Figure 3(a) shows the response function (Eq. 16) of the detection with $T_p = 120$ ns; $T_i = 10$ μs with a zoomed spectrum from 1 to 1.5 MHz in Fig. 3(b). Each discrete frequency component is a sinc^2 function whose width is inversely proportional to the camera exposure time T_e. It also shows that the Q factor, which is defined as the ratio between the central frequency and the pass band width, is very high for this lock-in detection. Usually the harmonic response of the lock-in detection is suppressed in a lock-in amplifier, but

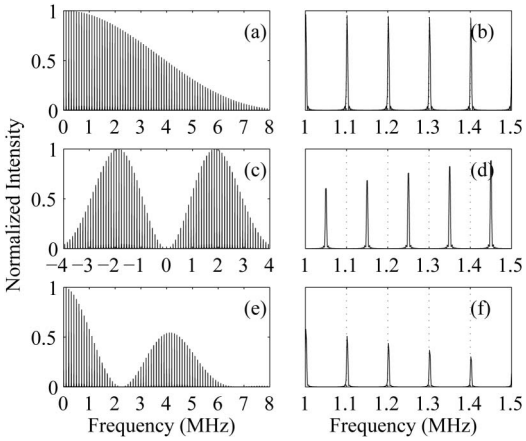

Fig. 3. (a) Harmonic response of the lock-in detection (f_i = 100 kHz, T_p = 120 ns); (b) zoom in at 1–1.5 MHz of (a); (c) spectrum of the light frequency shifted by US modulation (US pulse central frequency is 2.25 MHz); (d) zoom in at 1–1.5 MHz of (c); (e) spectrum of the time-varying fringes due to interference between US modulated light and reference beam (Δf = 2.25 MHz); and (f) zoom in at 1–1.5 MHz of (e).

here it is used to lock the wide spectrum of the single-cycle US modulation.

It should be noted that the minimum detected unmodulated signal [Eq. (5)] is provided at the midpoints of the frequencies shown in Fig. 3(b). However, given the high Q of the individual frequency components in practice (provided the frequency difference Δf between the signal and reference does not equal nf_i), then the unmodulated signal can be adequately canceled.

The spectrum of the US pulse train shown in Fig. 2 and described in the time domain by Eq. (15) is given by $A(f)\sum_0^\infty \delta[f-(n-1/2)f_i]$, where $n=0,1,2,\ldots$ and $A(f)$ is the normalized envelope of the spectrum. A delta function is used here, as the bandwidth of each frequency component is very narrow as discussed previously. The spectrum of the optical frequency shifted by these US bursts is

$$S(f)=A(f)\sum_{-\infty}^{\infty}\delta\left[f-\left(n+\frac{1}{2}\right)f_i\right], \tag{18}$$

where n is an integer, $A(f)=A(-f)$. Figures 3(c) and 3(d) show the spectrum of the frequency-shifted light [Eq. (18)] when US pulse width T_a = 444 ns (f_a = 2.25 MHz) and pulse time interval T_i = 10 μs. The frequency components shown in Figs. 3(c) and 3(d) cannot be detected directly and so need to be mixed with a reference beam at the detector plane.

Interfering the light described in Eq. (18) by the reference beam shifts the frequency components [Fig. 3(c)] by Δf to those shown in Figs. 3(e) and 3(f),

$$F(f)=\begin{cases}A(\Delta f+f)\sum\delta\left[\Delta f+f-\left(n+\frac{1}{2}\right)f_i\right], & \left(n+\frac{1}{2}\right)f_i\geq\Delta f\\ A(\Delta f-f)\sum\delta\left[\Delta f-f-\left(n+\frac{1}{2}\right)f_i\right], & \left(n+\frac{1}{2}\right)f_i<\Delta f\end{cases}, \tag{19}$$

where n is an integer. Substituting for Δf using Eq. (5) gives

$$F(f)=\begin{cases}A(\Delta f+f)\sum\delta\left[\left(n'+\frac{1}{2}\right)f_i+f-\left(n+\frac{1}{2}\right)f_i\right], & n\geq n'\\ A(\Delta f-f)\sum\delta\left[\left(n'+\frac{1}{2}\right)f_i-f-\left(n+\frac{1}{2}\right)f_i\right], & n<n'\end{cases}, \tag{20}$$

$$F(f)=\begin{cases}A(\Delta f+f)\sum\delta[-(n-n')f_i+f], & n\geq n'\\ A(\Delta f-f)\sum\delta[-(n-n')f_i-f], & n<n'\end{cases}, \tag{21}$$

where $n'=0,1,2,\ldots$, as described in Eq. (5). Therefore, it can be rewritten as

$$F(f)=\begin{cases}A(\Delta f+f)\sum\delta(-nf_i+f), & n=0,1,2,\ldots\\ A(\Delta f-f)\sum\delta(-nf_i-f), & n=-1,-2,-3,\ldots\end{cases}. \tag{22}$$

This indicates that the interference with the reference beam shifts the US modulated frequency by $-\Delta f$ and then flips the negative frequency to the positive part to become the temporal spectrum of the time-varying fringes. Figures 3(e) and 3(f) show the spectrum of the fringes that result from the interference between the modulated light with the spectrum shown in Fig. 3(c) and the reference beam with Δf = 2.25 MHz (Eq. 25). Recalling Eq. (17), it can be observed that the frequency components of the fringes match the pass band of the lock-in detection as shown in Figs. 3(b) and 3(f), resulting in efficient detection of the US modulated light.

In summary, unmodulated light can be eliminated if the laser pulse repetition rate f_i and frequency difference between the reference beam and incident beam Δf meet the condition described in Eq. 5, while US modulated light can be locked using a combination of phase-inverted US bursts synchronized with the laser pulses as shown in Fig. 2 [Eqs. (8) and (9)]. If required, e.g., for image comparison purposes, the unmodulated light frequency can be locked when $\Delta f = nf_i$.

B. Second Harmonic Implementation of Digital Heterodyne Holography

With minor modifications, the approach described in Section 2.A can be used to detect light modulated at the second harmonic US frequency while efficiently rejecting interference fringes due to unmodulated light and US modulated light at the fundamental frequency. It is important to make a distinction between the fundamental frequency and second harmonic discussed here and the harmonic content discussed in Section 2.A. In Section 2.A, the US modulated light contains harmonics at the pulse repetition frequency of the US pulse train (Fig. 3) when the US propagation is linear. In this section, the fundamental and second harmonic components refer to modulation due to nonlinear propagation of the US. Ultrasound wave distortion accumulates along its propagation path in the medium due to the sound wave propagation velocity being higher in a dense medium and lower in a rarefied medium. The degree of nonlinearity depends on the US pressure, medium properties, and propagation distance

[13]. Second harmonic US has been widely used in the clinical setting to enhance image contrast through the use of microbubbles [14]. Improvement in the lateral image resolution using second harmonic US generated through nonlinear propagation has also been reported [15]. This improvement is based on the fact that a narrower US beam waist with fewer sidelobes compared to the fundamental frequency can be obtained at higher harmonic US frequencies. Taking advantage of this, nonlinear US has also been applied to USMOT to improve the lateral imaging resolution [5,16], as the resolution of USMOT imaging is largely dependent on the US beam width. Significant US modulated second harmonic signal has been detected in our work when the US pressure is greater than 1 MPa in water. In this section, it is demonstrated that, by revising the US pulse train and the driving frequency difference Δf, the signal modulated by the second harmonic frequency of the US pulses can be extracted.

Analogous to the detection of the US modulation at the fundamental frequency (Section 2.A), the US in the second harmonic case is generated using a noninverted and inverted pulse pair (Fig. 4). The pulse sequence in Fig. 4 is shown distorted to represent the nonlinear propagation of the US.

To extract the second harmonic frequency component, the period of the laser pulse train is revised to $T_i' = T_i/2$ [laser pulse repetition rate $f_i' = 2f_i$ (Fig. 4 Laser)]. Therefore, as discussed in the fundamental case [Eq. (5)], the frequency difference Δf between the reference beam and incident beam should be

$$\Delta f = (2n+1)f_i, \qquad n = 0, 1, 2, \ldots, \tag{23}$$

where $f_i = 1/(2T_i)$ so that holographic fringes due to unmodulated light average out over the camera exposure time. Following Eq. (16), the pass band of the lock-in detection filter (given by the fast Fourier transform of the laser pulse series) shown in Fig. 4 is

$$P(f) = \mathrm{sinc}^2(\pi f T_p) \sum_0^\infty \delta(f - 2nf_i). \tag{24}$$

An example is shown in Figs. 5(a) and 5(b) (zoom in) for $T_i = 1/(2f_i) = 5$ μs, $T_p = 120$ ns. Figures 5(c) and 5(d) (zoom in) show the spectrum of the detected modulated light. The different frequency components are clear from looking at the positive part of the spectrum in Fig. 5(c). Modulation of the light by linear US propagation can be seen around 2.25 MHz along with the harmonic content at the pulse repetition frequency of the pulse train [Eq. (17)]. The second harmonic component due to nonlinear propagation of the US

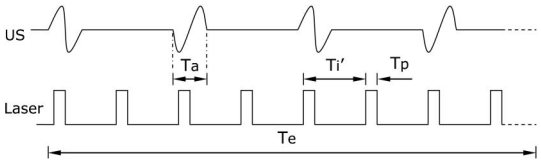

Fig. 4. Pulse sequences for second harmonic detection. US, noninverted and inverted US pulses; Laser, lock-in laser pulses. The US and laser are synchronized so that the US pulse arriving at the US focal zone modulates the light at the phases shown. T_a, US pulse duration; T_i', pulse train interval; T_p, laser pulse duration; T_e, exposure time.

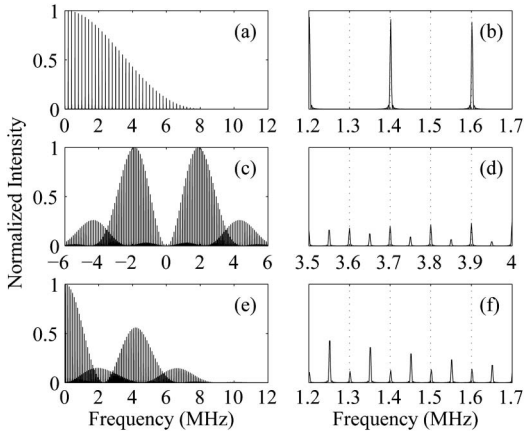

Fig. 5. (a) Harmonic response of the lock-in laser pulses ($T_i = 5$ μs, $T_p = 120$ ns); (b) zoom in (a) at 1.2–1.7 MHz; (c) frequency shift by the US with pulse central frequency at 2.25 MHz, pulse repetition rate $f_i = 100$ kHz; (d) zoom in (c) at 3.5–4 MHz; (e) frequency domain of interference signal between US modulated light and reference beam when $\Delta f = 2.3$ MHz; and (f) zoom in (e) at 1.2–1.7 MHz. The dashed vertical lines in (b), (d), and (f) indicate the position of the second harmonic frequency components which do not overlap with their fundamental counterparts.

occurs at around 4.5 MHz, along with its associated frequency content at the repetition frequency of the pulse train. Although the envelopes of the spectra appear to overlap, the distinct frequency components at multiples of the pulse repetition frequency do not.

Following the derivation in Section 2.A and replacing Δf in Eq. (25) with Eq. (23), the spectrum of the interference signal due to the fundamental US is given by

$$F(f) = \begin{cases} A(\Delta f + f) \sum \delta\left[-\left(n - \frac{1}{2}\right)f_i + f\right], & n = 1, 2, 3, \ldots \\ A(\Delta f - f) \sum \delta\left[-\left(n - \frac{1}{2}\right)f_i - f\right], & n = 0, -1, -2, \ldots \end{cases}. \tag{25}$$

For the second harmonic US modulation, the spectrum of the scattered light by the second harmonic US is

$$S'(f) = A'(f) \sum_{-\infty}^{\infty} \delta(f - nf_i), \tag{26}$$

where $A'(f)$ is the envelope of the second harmonic and n is an integer. Analogous to the analysis in the previous fundamental modulation case, the spectrum of the interference of the second harmonic US shifted light and the reference beam is

$$F(f) = \begin{cases} A(\Delta f + f) \sum \delta(\Delta f + f - nf_i), & nf_i \geq \Delta f \\ A(\Delta f - f) \sum \delta(\Delta f - f - nf_i), & nf_i < \Delta f \end{cases}, \tag{27}$$

$$F(f) = \begin{cases} A(\Delta f + f) \sum \delta[-(n - 2n' - 1)f_i + f], & n - 2n' - 1 \geq 0 \\ A(\Delta f - f) \sum \delta[-(n - 2n' - 1)f_i - f], & n - 2n' - 1 < 0 \end{cases}, \tag{28}$$

where n is an integer, $n' = 0, 1, 2, \ldots$. Therefore, it can be rewritten as

$$F(f) = \begin{cases} A(\Delta f + f) \sum \delta(-nf_i + f), & n = 0, 1, 2, \ldots \\ A(\Delta f - f) \sum \delta(-nf_i - f), & n = -1, -2, -3, \ldots \end{cases}. \tag{29}$$

The spectra of the fundamental [Eq. (25)] and the second harmonic [Eq. (29)] are shown in Figs. 5(e) ($\Delta f = 2.3$ MHz) and 5(f) (zoom in). Comparing Figs. 5(b) and 5(f), it can be seen that the fundamental frequency spectrum [without dashed line in Fig. 5(f)] doesn't match the response in Fig. 5(b). Compared with the lock-in response [Eq. (24)], half of the second harmonic frequency components are locked by the laser pulses as shown in Figs. 5(b) and 5(f) (dashed line), while the fundamental frequency components (without dashed line, shown in between the dashed lines) are filtered out.

3. EXPERIMENT

The experimental setup of the holography-based US modulated optical tomography is shown in Fig. 6. Continuous wave light from a laser (Oxxius Slim 50 mW, 532 nm wavelength) is split to two paths; one shifted by 80 MHz using an acousto-optic modulator AOM1 (Isomet 1205c-1, same as AOM2), while the other is shifted by 80 MHz + Δf by AOM2 and expanded as a reference beam. These driving signals are generated from each channel of function generator 1 (Tektronix AFG 3252, dual channel) and then gated by another channel (as in the pulse sequence shown in Figs. 2 and 4) from function generator 2 (Tektronix AFG 3022B dual channel) using two frequency mixers (Mini-Circuits ZEM-2B). The laser gating signal is synchronized with the US pulse train (Figs. 2 and 4 US) from the other channel of function generator 2. This US pulse train is then amplified by a RF power amplifier (Amplifier Research 75A250A) to drive a focused US transducer (Olympus A304S, 2.25 MHz, 48 mm focal length). When each US pulse propagates to the transducer focal point, the synchronized laser pulse is modulated at the US frequency. The scattered light exits from the aperture and then interferes with the reference laser beam, resulting in an interference speckle pattern on the CCD plane of the camera (Hamamatsu ORCA C4742-95-12ERG, 1344 × 1024 pixels, 12 bits, pixel size 6.45 μm × 6.45 μm). A 50 mm convex lens with its Fourier plane situated at the aperture is used to convert the hologram to the far field so that a sharp aperture image can be reconstructed. The distance between the lens and the camera is ~250 mm. The speckle size is then optimized by setting an appropriate aperture slit size (~2 mm). Practically, the aperture size is chosen such that the reconstructed aperture image is well separated from the zero order and low spatial frequency part of the image.

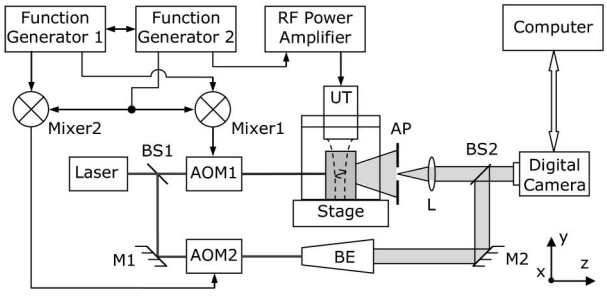

Fig. 6. Experimental setup. AP, aperture slit; BE, beam expander; BS1 and BS2, nonpolarized beam splitters; L, 50 mm lens; M1 and M2, mirrors; UT, ultrasound transducer.

In the fundamental frequency imaging experiment, a piece of chicken breast of 12 mm thickness, fixed by two glass slides and submerged in water, is scanned as a sample. Two optically absorbing objects ($x = 2$ mm, $y = 5$ mm) with 2 mm spacing [Fig. 7(b)] are embedded at the midplane. Both modulated and unmodulated light scattered by the sample transmit through the aperture, whose width and position are adjusted to make the reconstructed aperture image well separated from the zero-order and low-frequency part. The interval time of both laser and US pulses is 10 μs ($f_i = 100$ kHz), which ensures each pulse is well separated in the sample. The laser pulse width is 120 ns, which provides a broad enough harmonic response envelope for the US pulses and also maintains sufficient detected light intensity. Following the lock-in condition as derived in Eq. (5) for the modulated light, $\Delta f = 2.25$ MHz is set here while a strong unmodulated signal can be detected with $\Delta f = nf_i$, e.g., 2.3 MHz. This can be used for spatial resolution comparison purposes. Heterodyne holography is applied here to reduce the zero order effect and fixed pattern noise [3,17]. In this case, the camera frame rate is set to 4 fps and so the actual frequency difference between the reference beam and the signal of interest within the incident beam is $\Delta f' = \Delta f + 1$ Hz. Four images I1, I2, I3, and I4 are captured in sequence; and the aperture image is reconstructed by the Fourier transform of $(I1 - I3) + i(I2 - I4)$,

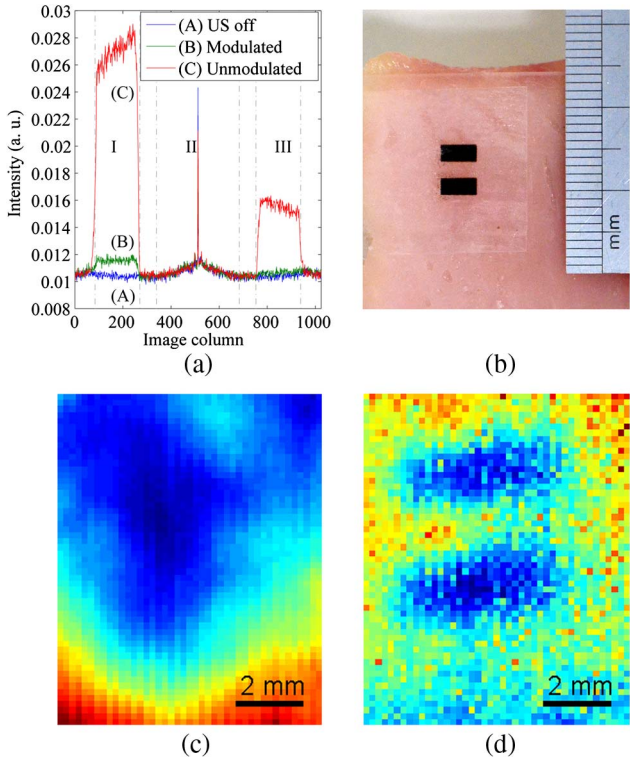

Fig. 7. (a) Comparison of cross sections of the reconstructed images of the aperture slit; (b) objects embedded into a piece of chicken breast; (c) DC image of the sample; and (d) AC image of the sample.

where i is the imaginary unit. The aperture to be imaged is extended to a slit in the y direction (in this case $x = \sim 2$ mm, $y = \sim 20$ mm) so that averaging can be performed along the y direction to reduce noise. This sample is scanned (step size 0.2 mm) in the y direction, then column by column in the x direction, to obtain a two-dimensional mapping of the US modulated signals.

The SNR for this experiment was insufficient to detect a second harmonic signal from the chicken breast, as its intensity is lower than that of the fundamental. However, to quantify the improvement on lateral resolution by locking at the second harmonic US modulation, an 18 mm thick tissue-mimicking phantom (scattering coefficient $\mu_s = 3.04$ mm^{-1}, anisotropy factor $g = 0.938$) with an optical absorbing edge embedded at the midplane is scanned with 0.2 mm per step in the x direction. DC, fundamental, and second harmonic images were obtained. The phantom consists of agarose (3%) and polystyrene microspheres (diameter = 1.6 μm). The anisotropy factor g is calculated according to Mie theory and μ_s by multiplying the particle density by the scattering cross section of the particle [18].

4. RESULTS

Figure 7(a) shows the reconstructed aperture image averaged over the rows for the fundamental frequency detection case and the chicken sample. This represents the k-space of the interference speckle pattern on the hologram plane and can be divided into three regions. Region I is the image of the aperture and corresponds to the spatial frequency content of the static fringes. (A) is the signal when US is off ($\Delta f = 2.25$ MHz); (B) is the US modulated signal ($\Delta f = 2.25$ MHz) and (C) shows the signal for the unmodulated signal (obtained by setting $\Delta f = 2.3$ MHz). Region II is the zero-order and low spatial frequency region and Region III is the conjugate image. Although the heterodyne holography technique should limit the presence of zero-order and conjugate images [17], they can still be observed in our experiment because of speckle decorrelation noise [11], system frequency drift, and motion artifacts. The two objects cannot be resolved in the DC light image [Fig. 7(c)], whereas the two objects are discernible in the US modulated image [Fig. 7(d)].

A comparison of the reconstructed aperture images for the gel phantom containing an absorbing edge is shown in Fig. 8 for fundamental and second harmonic US modulated light. In Fig. 8(a), the baseline of the second harmonic image is shifted to the same level as the fundamental to allow comparison. Region I shows the US modulated signal which, depending on the US pulse and laser pulse sequence, can be used to detect either the fundamental or second harmonic US modulated optical signal. Region II shows that the DC and that of the second harmonic is higher than the fundamental because laser pulse repetition rate for detecting the second harmonic (Fig. 4) is double that in fundamental detection (Fig. 2).

Modulation depths of both cases over the US pressure are also compared [Fig. 8(b)] and show that the second harmonic modulation becomes more significant at higher US pressure (>1 MPa) and increases faster than the fundamental modulation. This agrees with the trends of the second harmonic US case. In the results shown in Figs. 8(a), 8(c), and 8(d), the US peak–peak pressure is 2.4 MPa, allowing the second harmonic signal to be detected. The scans of the edge [Fig. 8(c)] with

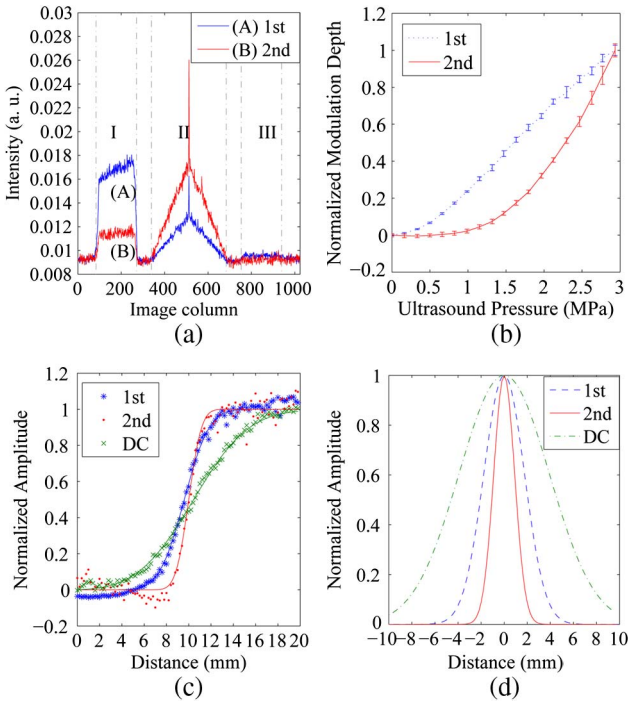

Fig. 8. (a) Reconstructed aperture images locked at the fundamental and the second harmonic frequency; (b) modulation depth of fundamental frequency modulation and second harmonic modulation with US pressure; (c) edge response functions of DC signal, fundamental modulation and second harmonic modulation; (d) line spread functions of (c).

fundamental modulation, second harmonic modulation, and DC light intensity show that higher lateral resolution can be obtained using the second harmonic modulation. Spatial resolution is estimated by least squared fitting to the edge response function as previously described in [19]. The corresponding line spread functions [Fig. 8(d)] show that the FWHM of the second harmonic modulation image is reduced from 9.6 mm (DC) to 4.1 mm (fundamental modulation) to 2.1 mm (second harmonic modulation).

5. DISCUSSION

Digital holography is a useful approach in the detection of US modulated light, as it provides amplification of the detected signal due to multiplication by a reference beam and also reduces the effects of speckle decorrelation due to unmodulated light and interference between unmodulated light and modulated light. Pulsed US is useful, as it can be used to obtain resolution along the acoustic axis and is compatible with commercial US scanners. Using pulsed US introduces multiple frequency components at the pulse repetition frequency into the modulated optical signal. Using a laser pulse sequence as multiple frequency lock-in detection provides a response in which the pass band of the detection is matched to the individual frequency components of the US modulated light. Although the overall bandwidth of the envelope is wide, the detection bandwidth of the individual frequency components is small (~5 MHz and 20 Hz, respectively, for the example in this experiment). This US pulse sequence is commonly used in pulse inversion US [14,15] and so is compatible with commercial scanners. There has been increasing interest in the application of digital holography to time reversal

techniques such as wavefront sensors [6,7]. The analysis provided here shows that the unmodulated light component can be canceled by appropriate setting of the pulse repetition frequency [Eq. (5)] independent of the US frequency, allowing the approach to be scalable to high frequency US. The analysis also demonstrates [Eq. (9)] that the maximum modulated light signal can be obtained using a sequence of pulses in which a pulse is followed by its inverted counterpart.

Modifying the pulse sequence allows second harmonic frequency components to be detected while suppressing the contribution of unmodulated light and light modulated at the fundamental US frequency. This provides improved lateral resolution, albeit at the expense of SNR. In practice, second harmonic US can be combined with microbubbles, which enhance the second harmonic signal due to nonlinear oscillation of the bubble. This will be applied in future work.

The theoretical derivation described was for the ideal case. It is therefore interesting to consider the effect of nonideal experimental conditions on the performance of the system. The shape of the laser pulse and US pulse determines the spectral envelope of the laser pulse train and US pulse train, and therefore it has relatively little effect on the ability of the system to match to the individual frequency components. This is determined by the interval time between the laser pulses and US pulses, which is therefore critical in the experiment. As in conventional US, the axial resolution of the system is reduced due to the finite bandwidth of the transducer. It should be also be noted that four frames of speckle pattern are required to implement heterodyne holography reconstruction, which means that speckle decorrelation between frames reduces SNR. This effect could be further reduced by using a high frame rate, high sensitivity camera in combination with a higher peak power pulsed laser.

6. CONCLUSION

A digital holography-based method is demonstrated for the detection of optical signals modulated by pulsed US. The method employs a series of US pulses comprised of a pulse followed by its inverted counterpart. These pulses are strobed by synchronized optical pulses, which produce a detection response analogous to a lock-in amplifier. Although the overall frequency content of the modulated light is broad, it consists of a series of discrete frequencies at the pulse repetition frequency which are matched by the detection response to provide efficient detection. The analysis demonstrates that the unmodulated light contribution to the detected signal can be canceled by appropriate selection of the pulse repetition frequency. It is also shown that the modulated signal can be maximized by selecting a pulse sequence which consists of a pulse followed by its inverted counterpart. By modifying the optical pulse sequence, the second harmonic content of the US modulated light can be extracted while filtering out contributions from the modulation at the fundamental frequency. This can be useful in improving lateral resolution and contrast. The technique is demonstrated in imaging absorbing objects embedded in a chicken breast and in a scattering gel phantom.

ACKNOWLEDGMENTS

This work was supported by the Biotechnology and Biological Sciences Research Council (BBSRC) UK (BB/F004826/1 and BB/F004923/1). H. R. was supported by the China Scholarship Council. Thanks to N. T. Huynh, D. He, and B. R. Hayes-Gill for helpful discussions.

REFERENCES

1. L. V. Wang, "Mechanisms of ultrasonic modulation of multiply scattered coherent light: an analytic model," Phys. Rev. Lett. **87**, 043903 (2001).
2. S. Leveque, A. C. Boccara, M. Lebec, and H. Saint-Jalmes, "Ultrasonic tagging of photon paths in scattering media: parallel speckle modulation processing," Opt. Lett. **24**, 181–183 (1999).
3. M. Gross, P. Goy, and M. Al-Koussa, "Shot-noise detection of ultrasound-tagged photons in ultrasound-modulated optical imaging," Opt. Lett. **28**, 2482–2485 (2003).
4. F. Ramaz, B. C. Forget, M. Atlan, A. C. Boccara, M. Gross, P. Delaye, and G. Roosen, "Photorefractive detection of tagged photons in ultrasound modulated optical tomography of thick biological tissues," Opt. Express **12**, 5469–5474 (2004).
5. H. Ruan, M. L. Mather, and S. P. Morgan, "Pulse inversion ultrasound modulated optical tomography," Opt. Lett. **37**, 1658–1660 (2012).
6. Y. M. Wang, B. Judkewitz, C. A. Dimarzio, and C. Yang, "Deep-tissue focal fluorescence imaging with digitally time-reversed ultrasound-encoded light," Nat. Commun. **3**, 928 (2012).
7. K. Si, R. Fiolka, and M. Cui, "Fluorescence imaging beyond the ballistic regime by ultrasound-pulse-guided digital phase conjugation," Nat. Photonics **6**, 657–661 (2012).
8. W. Leutz and G. Maret, "Ultrasonic modulation of multiply scattered light," Physica B **204**, 14–19 (1995).
9. S. Sakadzic and L. V. Wang, "High-resolution ultrasound-modulated optical tomography in biological tissue," Opt. Lett. **29**, 2770–2772 (2004).
10. Y. Li, H. Zhang, C. Kim, K. H. Wagner, P. Hemmer, and L. Wang, "Pulsed ultrasound-modulated optical tomography using spectral-hole burning as a narrowband spectral filter," Appl. Phys. Lett. **93**, 011111 (2008).
11. M. Atlan, B. C. Forget, F. Ramaz, A. C. Bocarra, and M. Gross, "Pulsed acousto-optics imaging in dynamic scattering media with heterodyne parallel speckle detection," Opt. Lett. **30**, 1360–1362 (2005).
12. L. Sui, R. A. Roy, C. A. DiMarzio, and T. W. Murray, "Imaging in diffuse media with pulsed-ultrasound-modulated light and the photorefractive effect," Appl. Opt. **44**, 4041–4048 (2005).
13. S. I. Aanonsen, T. Barkve, J. N. Tjotta, and S. Tjotta, "Distortion and harmonic generation in the nearfield of a finite amplitude sound beam," J. Acoust. Soc. Am. **75**, 749–768 (1984).
14. D. H. Simpson, C. T. Chin, and P. N. Burns, "Pulse inversion doppler: a new method for detecting nonlinear echoes from microbubbles contrast agents," IEEE Trans. Ultrason. Ferroelectr. Freq. Control **46**, 372–382 (1999).
15. B. Ward, A. C. Baker, and V. F. Humphrey, "Nonlinear propagation applied to the improvement of resolution in diagnostic medical ultrasound," J. Acoust. Soc. Am. **101**, 143–154 (1997).
16. J. Selb, L. Pottier, and A. C. Boccara, "Nonlinear effects in acousto-optic imaging," Opt. Lett. **27**, 918–920 (2002).
17. I. Yamaguchi and T. Zhang, "Phase-shifting digital holography," Opt. Lett. **22**, 1268–1270 (1997).
18. H. C. van de Hulst, *Light Scattering by Small Particles* (Dover, 1981).
19. S. M. Bentzen, "Evaluation of the spatial resolution of a CT scanner by direct analysis of the edge response function," Med. Phys. **10**, 579–581 (1983).